# An Intense, Quasi-Steady Thunderstorm over Mountainous Terrain. Part III: Doppler Radar Observations of the Turbulent Structure

KEVIN R. KNUPP AND WILLIAM R. COTTON

*Department of Atmospheric Science, Colorado State University, Fort Collins 80523*

(Manuscript received 18 February 1981, in final form 21 September 1981)

ABSTRACT

The evolution of the turbulent structure of an intense, quasi-steady thunderstorm is examined using Doppler radar estimates of turbulent kinetic energy dissipation rates ($\epsilon$) and radial shears of raw radial velocity ($\Delta V_r/\Delta R$). A comparison of turbulent patterns with mean storm airflow is made.

Observations taken during the quasi-steady mature stage reveal that turbulent intensity and activity peaked at mid to upper storm levels. The primary storm updraft was nearly turbulence-free at low levels, but exhibited increasingly turbulent activity at higher levels indicating a transition from quasi-laminar flow to bubble-like flow. Comparison of $\epsilon$ and $\Delta V_r/\Delta R$ patterns with environmental parameters such as equivalent potential temperature and momentum suggests that buoyancy and wind shear acted together to generate turbulent eddies, some greater than 500 m in size, at middle storm levels. At mid to upper storm levels, patterns of $\epsilon$ and $\Delta V_r/\Delta R$ exhibited considerable spatial and temporal variability, and maximum estimated dissipation rate estimates approached 0.15 $m^2 s^{-3}$. During one particular time period, 11 local $\epsilon$ maxima were estimated, some with magnitudes exceeding 0.07 $m^2 s^{-3}$.

## 1. Introduction

A commonly recognized feature of convective clouds is their highly variable and turbulent nature. Analog records of aircraft-measured vertical motion within cumulus clouds and thunderstorms (Warner, 1970, 1977; Byers and Braham, 1949; Sand, 1976) typically display a detailed structure, with small-scale turbulent variations superimposed on larger scale draft motions. Vertically and horizontally pointing Doppler radar observations (Battan, 1975, 1980; Battan and Theiss, 1973; Donaldson and Wexler, 1969) have revealed similar small-scale variations. These and other observations have disclosed that thunderstorm turbulence varies from very low magnitudes within low-level updrafts (Auer and Marwitz, 1968; Grandia and Marwitz, 1975) to extremely high magnitudes at mid to upper storm levels (Sand, 1976; Frisch and Strauch, 1976).

The presence of turbulence within storms quite likely has a significant impact on cloud physical and dynamical processes. When turbulence is present, mixing processes are enhanced, leading to increased spatial redistribution of heat, moisture and precipitation. Such mixing subsequently influences precipitation growth and increases entrainment of dry air into updrafts.

The purpose of this paper is to describe and explain the spatial patterns and temporal evolution of Doppler-radar-inferred turbulence within a quasi-steady thunderstorm. This storm occurred on 19 July 1977 over South Park, an elevated extensive valley region located in the central Colorado mountains, during the course of the month-long South Park Area Cumulus Experiment (SPACE). Analysis of this storm case study ranges from the mesoscale (Cotton *et al.*, 1982), to the storm scale (Knupp and Cotton, 1982), to the eddy or microscale (this paper). Storm and mesoscale measurement systems on this date included three Doppler radars (one C-band and two X-bands), 20 Portable Automated Mesonet (PAM) stations and one rawinsonde system. The location of the instrumentation is shown in Fig. 2 of Part I. Storm characteristics included organized downdraft circulations whose outflow gust front maintained a quasi-steady, anticyclonic and turbulent primary updraft. Updrafts attained peak speeds of ~25 m $s^{-1}$, and reflectivity factors exhibited peak magnitudes exceeding 60 dBZ. Specific characteristics of the mesoscale circulations leading to storm formation, and details of the storm kinematic structure, are given in Cotton *et al.* (1982) and Knupp and Cotton (1982), hereafter denoted as Part I and Part II, respectively.

## 2. Data and method of analysis

Doppler spectra variances and radial velocity estimates were obtained from a scanning X-band radar (NOAA-D) operated by the National Oceanic and Atmospheric Administration. The location of this radar is shown in Fig. 2 of Part I. Editing of variance

0022-4928/82/020359-10$06.50

estimates included deletion of points with signal-to-noise ratio (S/N) less than 8 dB, as well as deletion of points exhibiting a (spurious) variance value in excess of 40 $m^2s^{-2}$. Likewise, radial velocity estimates were thresholded at 5 dB S/N. Because of storm proximity and size, the radar scanning procedures provided only fair spatial resolution. Range gate spacing was 600 m, and successive beams were separated by 2.5° in azimuth and 1.5° in elevation, yielding a geometric mean distance between raw data points of 650 m at a range of 20 km. Raw "turbulence" data were interpolated to a three-dimensional Cartesian grid with 750 m horizontal spacing and 500 m vertical spacing using a spherical filter with 800 m radius. Points within the sphere were weighted linearly according to their distance from the center grid point. An average of 3–4 raw data points contributed to an individual Cartesian grid-point estimate.

In this study, the presence of turbulence is inferred from analysis of Doppler spectra and gate-to-gate variations of mean radial velocity ($\Delta V_r/\Delta R$). Analysis of storm turbulence using Doppler spectra has been done previously by Frisch and Strauch (1976). Both types of measurements are complementary in that Doppler spectra variances depict variable motions within a radar sample volume while absolute magnitudes of $\Delta V_r/\Delta R$ portray larger scale eddies. Comparison of the two measurements can also yield a qualitative check on the location and relative magnitude of storm turbulence.

The behavior of $\Delta V_r/\Delta R$ magnitudes is dependent on filtering effects produced by the radar pulse volume. Srivastava and Atlas (1974) have shown that variations in mean radial velocities due to turbulent fluctuations at scales small compared to the radar beamwidth are severely attenuated, while turbulent motions with scales much larger than the beamwidth are not filtered significantly. Thus, $\Delta V_r/\Delta R$ patterns throughout the storm will reflect different scales of turbulent motion due to the range dependence of the radar pulse volume. For the typical radar beam dimensions of this case (a transverse beamwidth of ~350 m and a pulse length of 150 m), the ratio of filtered to unfiltered energy (as estimated by first moment estimates) is ~2/3, assuming an outer inertial subrange scale of 2 km (see Fig. 4 in Srivastava and Atlas, 1974).

Both turbulent eddies and gradients of mean storm motions (~2 km scale) will contribute to radial shears of radial velocity. Inspection of smoothed (mean) radial velocity fields within the storm revealed maximum radial shears of $\sim 5 \times 10^{-3}$ $s^{-1}$. Typical average values were $< 2 \times 10^{-3}$ $s^{-1}$. In this paper, it is assumed that $\Delta V_r/\Delta R$ values (absolute values calculated from raw data) exceeding $5 \times 10^{-3}$ $s^{-1}$ are indicative of turbulent eddies.

Variance estimates [obtained by the Pulse Pair covariance technique (PPP)] were converted to the more range-normalized kinetic energy dissipation rate ($\epsilon$) using the formula

$$\epsilon \approx \frac{1.66}{R\theta}\left[\frac{\sigma_{11}^2}{1.26A}\right]^{1.5} \quad (1)$$

presented by Frisch and Clifford (1974). In (1), $\sigma_{11}^2$ is the second moment produced by turbulent fluctuations, $R$ is range, $\theta$ the one-way half-power beamwidth (0.8°), and $A$ the so-called universal constant. In their analysis, Frisch and Clifford used $A = 0.47$ which is approximately valid for one-dimensional spectra. Frisch and Strauch (1976) used a slightly higher value of $A = 0.53$ in their analysis of thunderstorm turbulence. The value of $A$ used in this study ($A = 1.44$), valid for three-dimensional turbulent spectra on which the conversion formula (1) depends, is obtained by multiplying the one-dimensional constant (0.47) by 55/18 (see Panchev, 1971, pp. 241–246). For the data presented in this paper, use of the three-dimensional constant reduces $\epsilon$ estimates to 19% of those computed using the one-dimensional constant.

The accuracy of $\epsilon$ estimates derived using (1) depends on several factors and assumptions. First, it is assumed that the turbulence being measured by the radar pulse volume is homogeneous and isotropic. Data presented here and elsewhere (e.g., Battan, 1980) suggest that the assumption of homogeneity may not rigorously hold within thunderstorms. Intuitively, it seems reasonable to expect that inhomogeneity and anisotropy would be greatest near regions of turbulence generation. Large inhomogeneous eddies generated by wind shear and density (buoyancy) fluctuations would tend to become more homogeneous and isotropic during transport from the source region. The sense of the error produced by anisotropy, for radars scanning at elevations <30°, would be an underestimate in $\epsilon$, assuming that anisotropy is mainly in the vertical direction. Errors produced by inhomogeneities of turbulence within the radar pulse volume are more difficult to estimate. Assessment of such errors would require application of a complicated numerical model, which is beyond the scope of this paper.

Second, it is assumed that the scales of turbulent motion within the radar pulse volume lie within the inertial subrange. The maximum physical beamwidth of 400 m should be within the outer scale of the inertial subrange for this case, but could not be verified. Third, it is assumed that turbulence is the primary contributor to Doppler spectrum variance. Other factors, such as wind shear and variations in precipitation fallspeed, also contribute to spectrum widening. The variance contribution from wind shear normal to the radial direction has been derived by Sloss and Atlas (1968). It is expressed as

$$\sigma_{st}^2 = (k_h^2 + k_v^2)(0.3R\theta)^2, \quad (2)$$

where $k_h$ and $k_v$ are the respective horizontal and vertical wind shear. The typical transverse shear contribution was found to be over an order of magnitude greater than contributions from radial shear ($k_r$), given by Sirmans and Doviak (1973) as

$$\sigma_{sr}^2 = (k_r h)^2/48,$$

where $h$ is the radar spatial pulse length. Inspection of smoothed (interpolated) radial velocity fields showed that shear-induced spectrum widening within the most highly sheared storm regions amounted to at most 1.2 $m^2 s^{-2}$ because of storm proximity. Observed maximum horizontal and vertical wind shears (obtained from "mean" interpolated fields) were both $10^{-2}$ $s^{-1}$, but large horizontal and vertical shears at the same point were uncommon. A shear of $10^{-2}$ $s^{-1}$ at a range of 20 km will produce a variance of 0.7 $m^2 s^{-2}$. More typical maximum transverse shear values fell in the range 5–8 $\times 10^{-3}$ $s^{-1}$, producing a variance (at $R$ = 20 km) of 0.4 $m^2 s^{-2}$. In the most severe cases, the transverse shear contribution amounted to ~15% of the total variance. In such a case, a variance error of 1 $m^2 s^{-2}$ in a total of 7 $m^2 s^{-2}$ will produce an $\epsilon$ error of ~20% at $R$ = 20 km.

The variance produced by variations in precipitation fallspeeds, given as $\sigma_p^2 = \sigma_D^2 \sin^2\alpha$, where $\alpha$ is the radar elevation angle and $\sigma_D^2$ the variance of particle fallspeeds, amounts to at most 0.30 $m^2 s^{-2}$ assuming $\sigma_D^2$ = 1 $m^2 s^{-2}$. Patterns of $\sigma_D^2$ will exhibit less spatial variation than those produced by wind shear, if large hail is absent.

Because the variances produced by precipitation and wind shear lay within the error range of PPP-derived Doppler spectra variances, the neglect of shear and precipitation effects leads to insignificant changes in the relative patterns of $\epsilon$ in this case study. This is substantiated by variance patterns, similar in magnitude and location, measured by the NOAA-C radar which was located in a position such that the large transverse wind shears seen by NOAA-D were absent, i.e., oriented perpendicular to its radial direction. In some storm regions $\epsilon$ values will be underestimated because of systematic biases in PPP variance estimates. Comparison of PPP-derived variances with those obtained by the maximum entropy method (MEM), considered to be a more accurate second-moment estimator (Sweezy, 1978), showed PPP estimates to be consistently lower (by as much as 1–3 $m^2 s^{-2}$) than MEM estimates.

In summary, the accuracy of Doppler-radar-derived $\epsilon$ estimates is dependent upon the accuracy of second-moment estimates and the assumptions made in the derivation of Eq. (1). An inflation of $\sigma_{11}^2$ due to wind shear is offset by underestimates of $\sigma_{11}^2$ as computed by the pulse pair covariance algorithm. The $\epsilon$ estimates calculated from Eq. (1) rely heavily on assumptions made, namely, that the turbulence is homogeneous and isotropic. While anisotropic turbulence probably leads to underestimates in $\epsilon$, the sense of $\epsilon$ errors produced by turbulence inhomogeneities is unknown.

In the following sections, the relative patterns of turbulence indicators are superimposed on the mean storm airflow patterns described in Part II. Because of potential inaccuracies in $\epsilon$ and $\Delta V_r/\Delta R$, only the relative variation in these quantities, not their absolute magnitudes, will be emphasized. Further, because dual-Doppler results were used, mean flow patterns may be subject to error in regions of high-magnitude hydrometeor vertical motion.

## 3. Mean storm-scale characteristics

The mean storm-scale characteristics and storm-environment interactions are summarized here. The storm of interest developed within an environment containing relatively low wind shear. However, within an hour after its formation, a mesoscale cold front moved into the region and significantly increased the low-level wind shear. This modified environment consisted of moist northerly flow capped by drier southerly wind at cloud levels. Vertical profiles of the environmental equivalent potential temperature ($\theta_e$) and the magnitude of vertical shear of the horizontal wind showed respective minimum and maximum values 3 and 1.5 km above the surface. A sounding representative of the storm's environment indicated 4 K of maximum buoyancy.

As a consequence of the modified environment, the storm was intense for a 90 min period (1830–2000 MDT), assumed quasi-steady circulations for a 45 min period (1845–1930 MDT), and moved 40–50° to the left of the cloud-level environmental flow. During the quasi-steady period two updrafts were present. A primary updraft was located in the northwest (downshear) storm quadrant and attained peak vertical speeds of ~25 m $s^{-1}$. A secondary, weaker (10–20 m $s^{-1}$) and less steady updraft was located in the southern (upshear) quadrant. This updraft is not shown in the analysis presented herein, but is visible in Figs. 6b and c of Part II. The Doppler analyses suggested the presence of several downdraft branches. The most significant downdrafts were situated in the southeast–southwest storm quadrants where relative inflow of low-valued $\theta_e$ produced evaporation of cloud and precipitation particles. These downdrafts were confined primarily to the lower levels and attained peak estimated speeds of ~10 m $s^{-1}$.

The interaction of storm and environmental flow fields produced highest vector lateral wind shears along the western storm flank. The magnitude of the vector lateral wind shear is defined here as $[(\partial w/\partial x)^2 + (\partial w/\partial y)^2 + (\partial u/\partial z)^2 + (\partial v/\partial z)^2]^{1/2}$. These shears

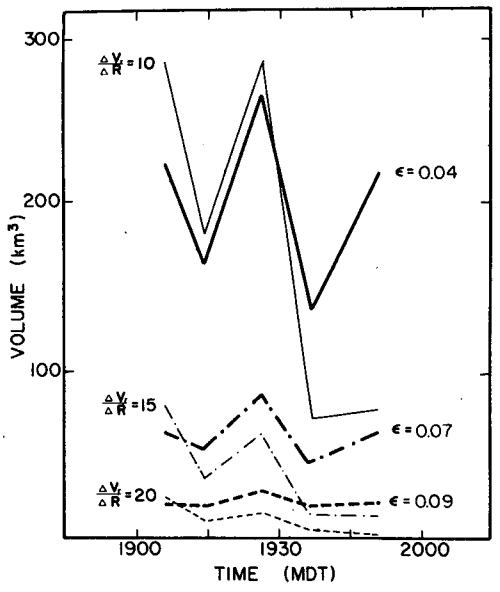


FIG. 1. Approximate volumes contained by various $\epsilon$ and $\Delta V_r/\Delta R$ surfaces as a function of time. Thin lines represent labeled $\Delta V_r/\Delta R$ ($10^{-3}$ s$^{-1}$) volumes, thick lines depict labeled $\epsilon$ (m$^2$ s$^{-3}$) volumes.

were greatest at upper midlevels where the environmental winds and storm updrafts attained greatest magnitudes. The reader is referred to Part II for more explicit details concerning the mean storm characteristics and storm-environment interactions.

## 4. Sources and sinks of turbulent energy

A simplified form of the turbulent kinetic energy (TKE) equation can be expressed in tensor form as

$$\frac{\partial \bar{e}}{\partial t} = \underbrace{-U_j \frac{\partial \bar{e}}{\partial x_j}}_{\text{(a)}} \quad \underbrace{-\overline{m_i'' U_j''} \frac{\partial \bar{U}_i}{\partial x_j}}_{\text{(b)}} \quad \underbrace{-\frac{\partial}{\partial x_j}(\overline{eU_j''})}_{\text{(c)}}$$

$$\underbrace{-\frac{\partial}{\partial x_j}(\overline{U_j'' p''})}_{\text{(d)}} \quad \underbrace{-g\overline{\rho'' U_j''}\delta_{j3}}_{\text{(e)}} \quad \underbrace{-\rho_0 \epsilon}_{\text{(f)}}, \qquad (3)$$

where $\bar{e} = \frac{1}{2}\rho_0 U_j''^2$ is the turbulent kinetic energy, $m_i'' = \rho_0 U_i''$ is the turbulent momentum, $\rho$ is density, $U_k$ are the velocity components and $p$ is pressure. Double-primed quantities denote deviations from an average quantity, i.e., $p'' = p - \bar{p} = p - (p_0 + p')$. Subscript $-$ zero quantities represent a basic reference state which varies in height only. Eq. (3) equates the local rate of change of turbulent kinetic energy with (a) transport by mean flow fields, (b) mechanical production (wind shear), (c) transport by turbulence, (d) pressure-velocity correlations, (e) buoyant production, and (f) molecular dissipation ($\epsilon$).

The TKE budget within cumulonimbi has never been determined. The interpretation of Eq. (3) is greatly simplified if the redistribution terms (c) and (d) are assumed small compared to terms (a), (b), (e) and (f). Circumstantial evidence supporting this assumption is provided by turbulence spectra obtained by aircraft within cumulus congestus clouds of 1–4.5 km depth (MacPherson and Isaac, 1977) and within severe cumulonimbi (Steiner and Rhyne, 1962). These spectra show an approximate $-5/3$ slope between 100 and 400 m for cumulus congestus and 100 and 500–1000 m for severe cumulonimbi, suggesting that a balance may be present between generation and dissipation of TKE within these length intervals. If we further assume that the TKE is in a steady state following the motion ($D\bar{e}/Dt = \partial\bar{e}/\partial t + U_j \partial\bar{e}/\partial x_j = 0$), then TKE dissipation [term (f)] may be equated to TKE generation [terms (b) and (e)].

## 5. Temporal evolution of $\epsilon$ and $\Delta V_r/\Delta R$

The temporal behavior of storm turbulent activity is illustrated in Fig. 1, which depicts the volume contained by specific $\epsilon$ and $\Delta V_r/\Delta R$ constant surfaces. Radial velocity gradients or fluctuations exhibit a temporal oscillation prior to declining sharply after 1927 (all times MDT). This diminution was concurrent with decreased storm vigor and change in storm structure from unicellular to multicellular. Corresponding temporal changes in dissipation rate volumes exhibit a fluctuating behavior throughout, but with no persistent sharp decrease after 1927. Such a pattern suggests that large turbulent eddies (and wind gradients) became less prominent, but that smaller scale turbulent motions remained relatively active throughout the analysis period. The fluctuating behavior of both radial velocity gradients and dissipation rates apparently indicates the impulsive, nonsteady nature of the storm at scales $\leqslant 2$ km. Such a behavior was much less prominent in the analysis of mean motions (Knupp and Cotton, 1982). According to Fig. 1, turbulent activity was most substantial at 1907 and 1927.

Fig. 2 is a composite of vertical profiles of areas contained by specific $\epsilon$ and $\Delta V_r/\Delta R$ contours during the intense unicellular (1907, 1915, 1927) and somewhat weaker subsequent multicellular (1937, 1951) storm stages. These profiles depict, as does Fig. 1, the decrease in storm turbulent activity after 1927. During the intense stages, $\Delta V_r/\Delta R$ profiles exhibit a primary peak at 3–6 km AGL and a secondary peak at 10 km AGL. Corresponding $\epsilon$ profiles reveal a striking minimum near 2 km AGL, and a prominent peak at 9 km, ~4 km above the $\Delta V_r/\Delta R$ peak. The relative maximum in $\epsilon$ near the surface is probably the result of spectrum widening produced by ground clutter. Vertical profiles during latter storm stages exhibit decreased magnitudes at most levels.

The decline of $\Delta V_r/\Delta R$ with time is especially striking (because the storm was not completely scanned in 1937 and 1951, these values are somewhat underestimated).

The difference in $\Delta V_r/\Delta R$ profiles in Fig. 2 suggests the presence of larger mean wind gradients and greater activity of large turbulent eddies during 1907–1927. The fact that $\epsilon$ areas exhibit a maximum ~4 km above the corresponding $\Delta V_r/\Delta R$ maximum during 1907–1927 implies a cascading of large eddies, generated at mid-levels within regions of high wind shear and concurrent significant entrainment, were subsequently transported vertically within the updraft(s) while the turbulence was slowly cascading to smaller scales.

## 6. Spatial patterns of turbulence

Patterns of $\epsilon$ and $\Delta V_r/\Delta R$ from selected horizontal and vertical planes are displayed in Figs. 3–5. An example of low-level $\epsilon$ patterns is shown in Fig. 3 for 1907. Largest $\epsilon$ magnitudes in the eastern storm quadrant are located near a confluent flow region and are associated with an inferred downdraft circulation. This downdraft feature was inferred from multiple-Doppler radar analyses not presented. Another feature which consistently appeared at this level was the low turbulent activity ($\epsilon \leqslant 0.009$ m$^2$ s$^{-3}$) within the inflow sector northwest of the reflectivity core (precipitation within the low-level updraft allowed it to be observed by radar). This observation is consistent with aircraft measurements which often indicate low turbulence at low levels within updrafts of northeast Colorado thunderstorms (e.g., Grandia and Marwitz, 1975).

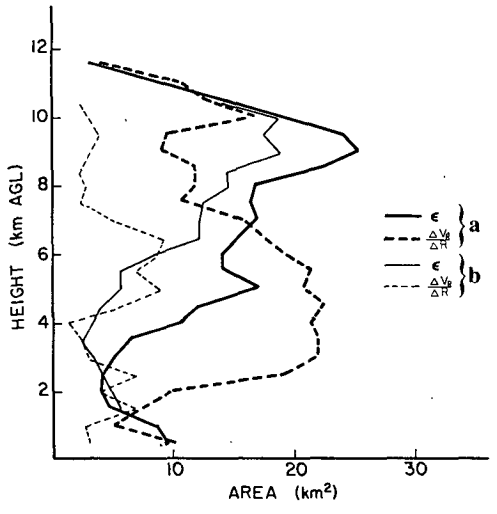


FIG. 2. Vertical profiles of horizontal areas contained by $\epsilon = 0.04$ m$^2$ s$^{-3}$ contours (solid lines) and $\Delta V_r/\Delta R$ ($10^{-2}$ s$^{-1}$) contours (dashed lines), composited for the 1907, 1915 and 1927 scans (a), and for the 1937 and 1951 scans (b). Add 3 km for height above MSL.

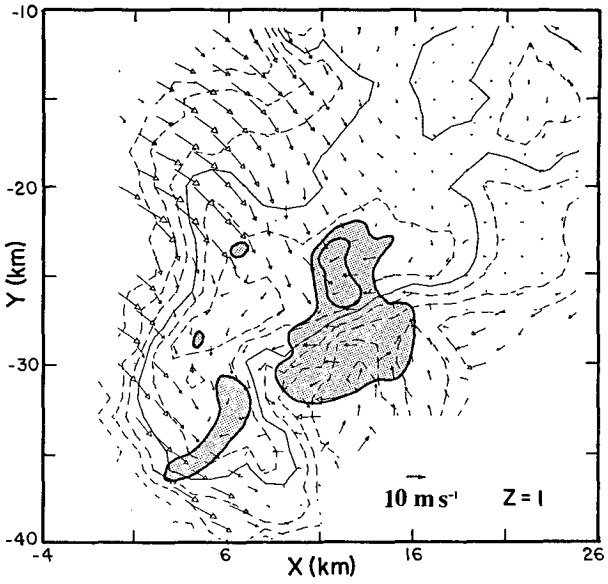


FIG. 3. Patterns of reflectivity factor, mean wind vectors (storm relative) and dissipation rate estimates at 1 km AGL at 1907 MDT. Reflectivity contours (thin solid and dashed lines) are drawn every 5 dBZ, with 30 dBZ solid. Dissipation rate contours are drawn at 0.02 and 0.04 m$^2$ s$^{-3}$. The NOAA-D radar is located at the coordinate origin.

Turbulent patterns at lower midlevels (4 km AGL) at 1927 are shown in Figs. 4 and 5. Here turbulent activity was most substantial along the western and southwestern regions of the storm. Especially noteworthy are the zones of high $\epsilon$ and $\Delta V_r/\Delta R$ illustrated in Figs. 4c and 5c. These lower mid-level zones of turbulence are coincident with the regions of entrainment and downdraft initiation downshear of the southern flank updraft. Such patterns suggest that relative inflow of dry environmental air, in addition to wind shear in the updraft vicinity, generated turbulence by buoyant and mechanical production, respectively. The weak flow region on the downshear side (north and east) of the reflectivity core at 4 km AGL consistently exhibited very low turbulence. At upper mid-levels ($z$ = 7, Figs. 4b and 5b) estimated turbulent patterns varied in time and space. Greatest $\epsilon$ and $\Delta V_r/\Delta R$ values were associated with large transverse wind shears. The considerable number of local maxima exceeding 0.04 m$^2$ s$^{-3}$ is particularly striking at 1927. Corresponding $\Delta V_r/\Delta R$ patterns in Fig. 5 showed less variability. Relatively high-speed flow west of the updraft at 7 km was virtually turbulence free. At upper levels, where dissipation rates <0.01 m$^2$ s$^{-3}$ were relatively rare, the location of greatest turbulent activity varied with time.

Correlations of $\Delta V_r/\Delta R$ with $\epsilon$ (Figs. 4 and 5) are especially high on the 1927 MDT $z$ = 7 and $x$ = 0 planes within the more turbulent regions. Based on these observations and the results of the study by Srivastava and Atlas (1974), the scale of turbulence

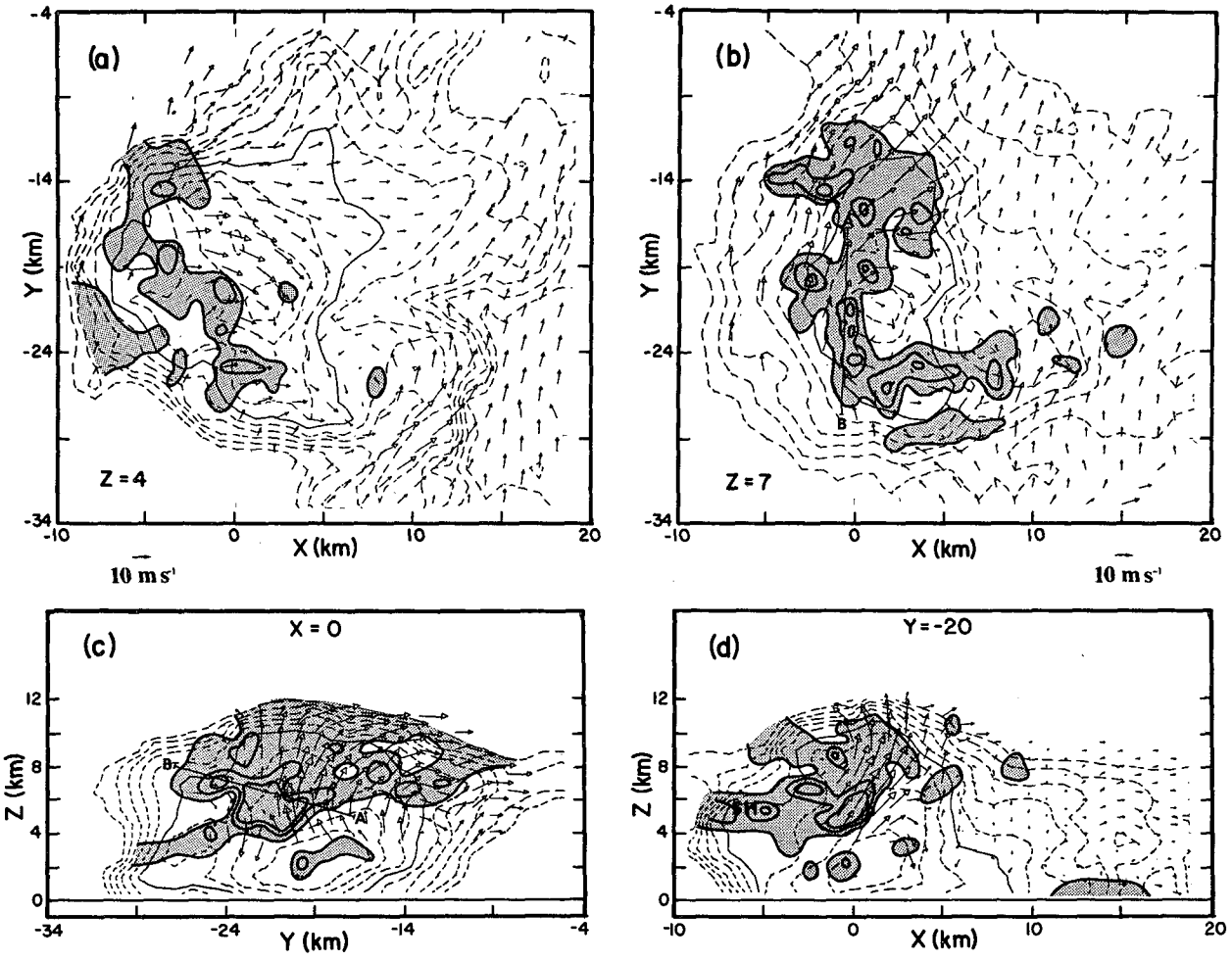


FIG. 4. Patterns of reflectivity factor, mean wind vectors (storm relative) and dissipation rate estimates at 1927 MDT for selected horizontal and vertical planes. Reflectivity contours as in Fig. 3. Contours of $\epsilon$ are drawn for $\epsilon$ = 0.02, 0.04 and 0.07 m$^2$ s$^{-3}$. The NOAA-D radar is located at the coordinate origin.

can be estimated. At the range involved here, the width of the radar beam (one-way half-power) varies from 170 m at $R$ = 12 km ($y$ = −12) to 380 m at $R$ = 27 km ($y$ = −27). Thus, the intense turbulent core visible near $y$ = −22 ($R$ = 22) on the $x$ = 0 vertical plane in Figs. 4 and 5 indicates significant turbulent energy at scales both smaller than 500 m and larger than 500 m. Turbulent eddies <500 m are indicated by small-scale motions within the radar sample volume which contribute to Doppler spectrum variance, and hence large values of $\epsilon$ (Fig. 4). Eddies >500 m are indicated by $\Delta V_r/\Delta R$ (Fig. 5) which are not significantly filtered for a beamwidth of 310 m.

In other areas where turbulence was more localized, correlations were less direct. In some cases, relatively high $\epsilon$ or $\Delta V_r/\Delta R$ were not accompanied by the other. Battan and Theiss (1973) noted similar decorrelations between magnitudes of Doppler spectra variances and $\Delta V_r/\Delta R$. Such a behavior may indicate variations in the size scale of turbulent motion.

An interesting pattern appears on the $y$ = −20 plane of Fig. 4d. A relatively narrow zone of high $\epsilon$ extends westward from the turbulent updraft core at mid-levels. This pattern, also present at earlier times, was associated with relatively strong vertical shear of the horizontal wind that could be seen in the individual radar scans. The large shears may have been a consequence of the near co-location of the sloping primary updraft transporting northerly momentum to that region and mid-level southerly flow diverging around the primary updraft. There also is some suggestion that semi-discrete cellular growth in this region contributed to the shear. As a result, turbulence was generated near the sheared region (labeled SH) separating the updraft horizontal flow from the enhanced environmental southerly flow. The sheared region SH is not evident in Figs. 4 and 5, but can be seen in Fig. 7 of Part II.

Although the smoothed $\epsilon$ patterns displayed in Fig. 4 exhibit considerable spatial variability, raw $\sigma^2$ (Doppler spectra variance) and $V_r$ (radial velocity)

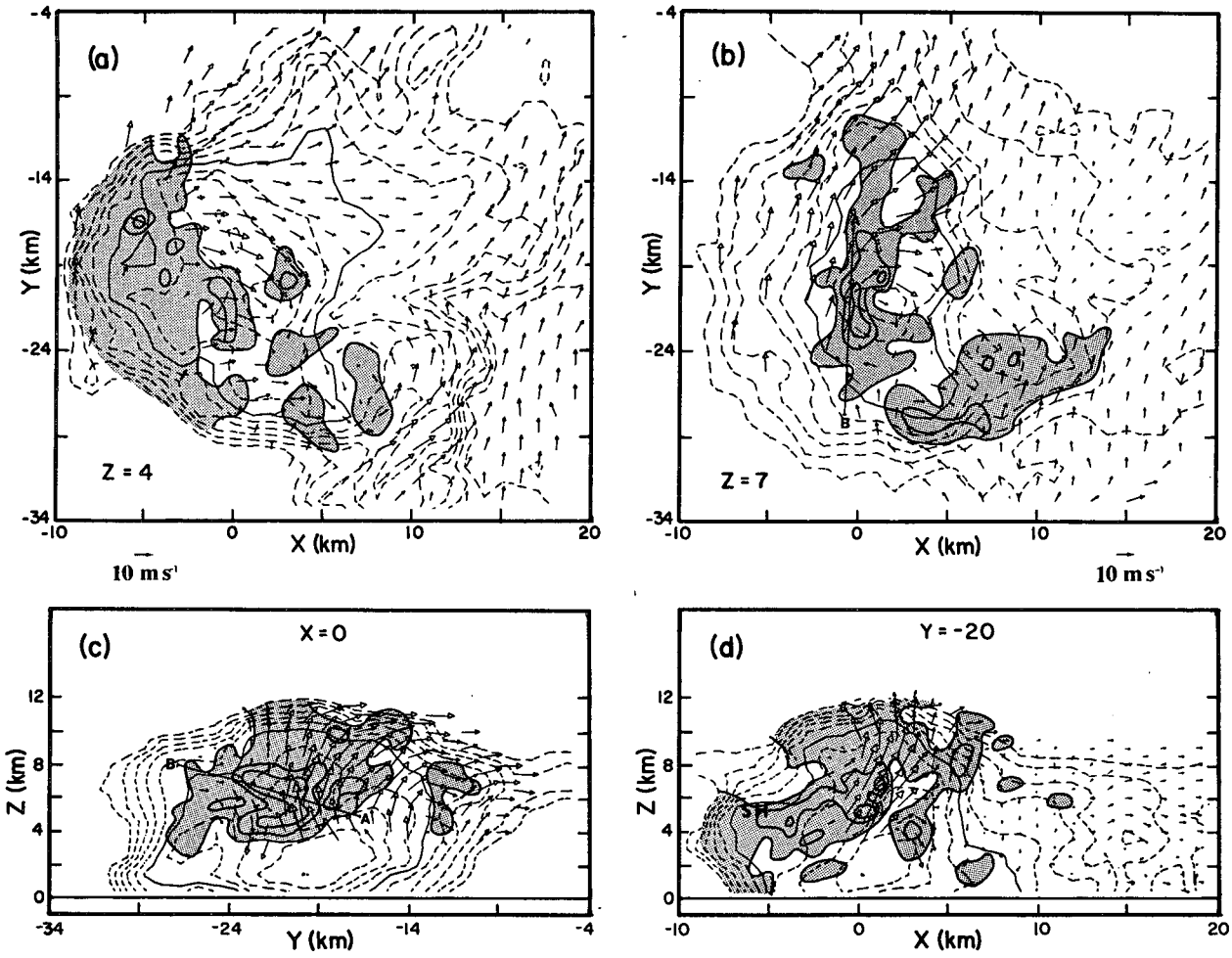


FIG. 5. Patterns of reflectivity factor, mean wind vectors (storm relative) and radial velocity differences ($\Delta V_r/\Delta R$) at 1927. $\Delta V_r/\Delta R$ contours are drawn at $5 \times 10^{-3}$, $10 \times 10^{-3}$ and $15 \times 10^{-3}$ $s^{-1}$. The NOAA-D radar is located at the coordinate origin.

data reveal even greater variability. Table 1 presents radial velocity, variance, and returned power estimates from successive range gates (600 m spacing) through one of the storm's most turbulent portions at 1927. The straight solid line (AB) drawn in Figs. 4b, 4c, 5b and 5c indicates the projection of this radial segment onto nearby horizontal and vertical planes. Variance and radial velocity estimates listed in Table 1 exhibit extreme gate-to-gate variations. Although numerous high variances occur, surprisingly low values are also present. The fluctuating behavior of radial velocities [up to 20 m $s^{-1}$ (600 m)$^{-1}$] implies relatively large-scale and intense turbulent eddies. Variation of successive variance estimates presumably results from extreme wind shears and smaller scale turbulence bordering individual eddies. Similar fine-scale variations in $\sigma^2$ and $V_r$ have been presented in vertically pointing Doppler data (Battan, 1975, 1980), indicating that such variations may be found along the horizontal or vertical direction.

## 7. The relationship between storm-environment interactions and storm turbulence

Turbulence within this storm appears to have been generated by both mechanical and buoyant production. Because wind shear and entrainment (both dynamic and turbulent) are closely related, the relative contribution made by each is difficult to assess. An analysis of the environmental wind shear (Fig. 2, Part II) showed little correlation between regions of active storm turbulence and ambient wind shear. However, based on inferences from the three-dimensional cloud model experiments reported by Tripoli and Cotton (1980), three storm-environmental parameters are proposed which should be indicative of the potential for shear and buoyancy production of turbulence. These parameters are: 1) the difference between storm and environmental horizontal momentum; 2) updraft momentum flux and its vertical divergence; and 3) minimum values of environmental equivalent potential temperature ($\theta_e$).

TABLE 1. Estimates of radial velocity, variance and returned power from successive range gates along line AB in Figs. 4 and 5. The measurements are from the radar beam with azimuth = 181.5° and elevation = 17.0°.

| Gate | $z$ (km) | $R$ (km) | $V_r$ (m s$^{-1}$) | $\sigma^2$ (m$^2$ s$^{-2}$) | S/N (dB) |
|---|---|---|---|---|---|
| 14 | 5.14 | 16.8 | −4.9 | 4.5 | 32 |
| 15 | 5.32 | 17.4 | −6.7 | 2.9 | 33 |
| 16 | 5.50 | 18.0 | −5.8 | 3.4 | 29 |
| 17 | 5.69 | 18.6 | −6.6 | 6.4 | 24 |
| 18 | 5.87 | 19.2 | −0.8 | 1.7 | 28 |
| 19 | 6.05 | 19.8 | −13.9 | 12.6 | 28 |
| 20 | 6.24 | 20.4 | 10.9 | 19.7 | 31 |
| 21 | 6.42 | 21.0 | 8.6 | 4.6 | 28 |
| 22 | 6.60 | 21.6 | −3.1 | 2.8 | 30 |
| 23 | 6.79 | 22.2 | −14.0 | 39.2 | 32 |
| 24 | 6.97 | 22.8 | −2.3 | 3.4 | 31 |
| 25 | 7.15 | 23.4 | −9.6 | 22.8 | 26 |
| 26 | 7.34 | 24.0 | 2.6 | 6.9 | 26 |
| 27 | 7.52 | 24.6 | 15.0 | 16.3 | 26 |
| 28 | 7.70 | 25.2 | −6.2 | 25.9 | 23 |
| 29 | 7.89 | 25.8 | −13.4 | 8.3 | 23 |
| 30 | 8.07 | 26.4 | −9.8 | 11.2 | 19 |
| 31 | 8.25 | 27.0 | −8.7 | 6.0 | 18 |
| 32 | 8.44 | 27.6 | −9.7 | 5.8 | 17 |

Fig. 6a shows the magnitude of the difference between storm inflow horizontal momentum ($\rho_0 \mathbf{V}_0$) and environmental horizontal momentum ($\rho_z \mathbf{V}_z$), $|\rho_0 \mathbf{V}_0 - \rho_z \mathbf{V}_z|$, where zero subscripts denote inflow quantities and $z$ subscripts represent environmental quantities as a function of height. Assuming conservation of horizontal momentum within the updraft, the profile of Fig. 6a would represent storm-environmental differences in horizontal momentum. However, the presence of turbulent and dynamic entrainment and pressure gradient forces will reduce such momentum differences, and thus produce deviations between the actual profile and Fig. 6a profile which increase with height. Large values of $|\rho_0 \mathbf{V}_0 - \rho_z \mathbf{V}_z|$ should be indicative of the potential for creating:

1) Diversion of the ambient flow ($\mathbf{V}_z$) about updrafts and creation of inflow entrainment into the wake low-pressure zone on the downshear side of the updraft. This process has been modeled by Tripoli and Cotton (1980) and inferred from observation by Heymsfield *et al.* (1978).

2) Local regions of strong vertical shear as a consequence of interactions with a sloping updraft.

Fig. 6a indicates that the primary maximum in $|\rho_0 \mathbf{V}_0 - \rho_z \mathbf{V}_z|$ occurs at a height of 3 km AGL, with a secondary maximum occurring at a height of 6 km AGL.

Also shown in Fig. 6a is the vertical profile of peak updraft mass flux ($\rho_z w_z$). Because data were unavailable at levels under $z = 4$, updraft magnitudes were estimated as follows: at cloud base ($z = 1$) a peak updraft of 7 m s$^{-1}$ was assumed, which is consistent with cloud-base updraft measurements obtained by aircraft in northeast Colorado (e.g., Grandia and Marwitz, 1975). The peak updraft at $z = 2.5$ was obtained by interpolation between the estimate at $z = 1$ and the Doppler measurements at $z = 4$. Large values of $\rho_z w_z$ imply the existence of substantial lateral shear between the updraft and a relatively quiescent environment. Moreover, by mass continuity considerations, strong vertical divergence of $\rho_z w_z$ implies that a strong horizontal convergence (or dynamic entrainment) in the updraft must be present, assuming that $\rho_z w_z$ is vertically stacked. In reality, updrafts exhibit a slope, thus producing peak updraft mass fluxes which are only approximately vertically stacked from level to level. The maximum

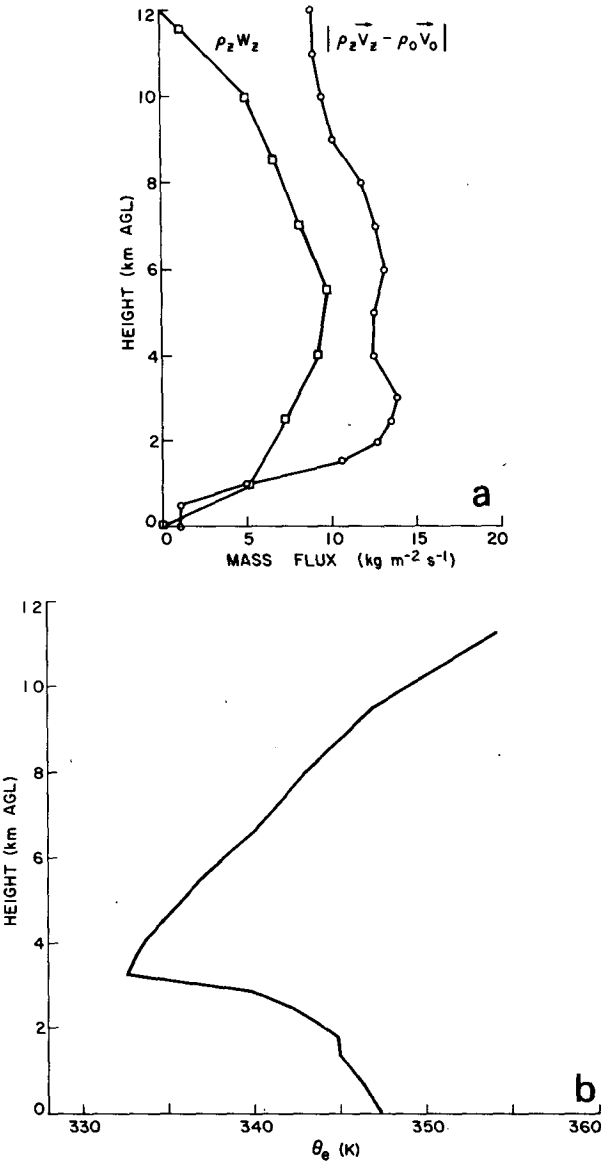


FIG. 6. Vertical profiles of (a) the magnitude of the difference between low-level momentum ($\rho_0 \mathbf{V}_0$) and environmental momentum at cloud levels ($\rho_z \mathbf{V}_z$), $|\rho_0 \mathbf{V}_0 - \rho_z \mathbf{V}_z|$, and the maximum updraft mass flux ($\rho_z w_z$) at 1927 MDT; (b) environmental equivalent potential temperature ($\theta_e$). Add 3 km for height above MSL.

of $\rho_z w_z$ occurs in the layer between 4 and 6 km AGL. The largest divergence of $\rho_z w_z$ in the cloud layer is between 1 and 4 km AGL. Above 6 km AGL, the convergence of $\rho_z w_z$ implies that detrainment from the updraft should be prevalent.

Fig. 6b shows the vertical profile of environmental equivalent potential temperature ($\theta_e$). Minimum values of $\theta_e$ should correspond to the largest thermodynamic consequences of entrainment and, therefore, the potential for buoyancy production of turbulence. As can be seen in Fig. 6b, the minimum $\theta_e$ occurs at 3 km AGL, with relatively small values of $\theta_e$ occurring throughout the layer from 2 to 7 km AGL.

Thus, Fig. 6a suggests that the large differences between environmental momentum and storm updraft momentum (both horizontal and vertical), as well as strong divergence of vertical mass flux in the 2–7 km AGL layer, provide strong dynamic forcing for the intrusion of low-valued $\theta_e$ air into the storm. The significance of this low-valued $\theta_e$ air is twofold. Some of this air participates in the formation of penetrative downdrafts, described in Part II, which may enhance horizontal shear of vertical winds, consequently increasing turbulence production. The low-valued $\theta_e$ air also contributes to buoyancy generation of turbulent kinetic energy (TKE) through the production of density fluctuations as a consequence of the mixing of condensing and evaporating air parcels.

Comparison of the Fig. 6 profiles with the observed profiles of turbulence indicators ($\epsilon$ and $\Delta V_r/\Delta R$, Fig. 2) yields the following scenario. Dynamic entrainment, which peaked between 2 and 6 km AGL, and storm-environment momentum differences which peaked between 2 and 7 km AGL, combined to generate TKE by buoyant and shear production. Consequently, TKE generation would have been most substantial between 2 and 7 km AGL. This is in surprisingly good agreement with the $\Delta V_r/\Delta R$ profile of Fig. 2 (bold dashed line, intense storm stage) which reveals a maximum between 2 and 6 km AGL. (Similar arguments could be applied to other storm environments which have a significant mid-level $\theta_e$ minimum.) As shown in Figs. 4 and 5, the mean Doppler velocity patterns reveal an organized flow into the storm and an inferred turbulent eddy structure along the southern and western boundaries of the storm. These "turbulent" eddies are depicted by $\Delta V_r/\Delta R$ patterns. [At the ranges for this case, eddies larger than 500 m would not be significantly filtered from $\Delta V_r/\Delta R$ patterns. See Section 2 and Srivastava and Atlas (1974).]

Fig. 2 also reveals that the peak in $\epsilon$ estimates was more prevalent at higher levels, suggesting a dominance of smaller scale eddy motions in that region. Comparison of the spatial distributions of $\epsilon$ and $\Delta V_r/\Delta R$ with the expected interval in which TKE generation should occur, however, reveals that at 1927 (Figs. 4 and 5) both large- and small-scale turbulence exhibited peak magnitudes between 4 and 8 km AGL. The implication is that shear- and buoyancy-generated eddies occurred over a broad range of scales. These eddies reached their peak intensities between 4 and 8 km AGL. At higher levels in the cloud, turbulence was diffused through a greater areal extent of the cloud and eventually cascaded to smaller scales.

During later time periods, the magnitude and areal extent of $\epsilon$ and $\Delta V_r/\Delta R$ exhibited lower values. This decrease in turbulent intensity was associated with significantly lower magnitudes of horizontal and vertical shears of mean storm airflow.

## 8. Discussion and summary

The turbulence data presented here have revealed large magnitudes of turbulent energy and considerable variability occurring on scales smaller than 2 km. Measured radial velocity patterns exhibited extreme and nonsystematic variations throughout the storm's turbulent portions. Corresponding variations in Doppler spectra variance estimates also revealed outstanding large-scale and small-scale variations.

The variability of radial velocity and Doppler spectra variance estimates has previously been measured primarily with nonscanning Doppler radars. Vertically pointing Doppler radar data presented by Battan (1975, 1980), Battan and Theiss (1973) and Donaldson and Wexler (1969) have revealed significant variations in Doppler spectra variance and radial velocity fields over distances of a few hundred meters. Similar fine-scale patterns have been observed in the horizontally pointing measurements of Battan and Theiss (1973), as well as the data presented in Section 5. These patterns seem to indicate that substantial inhomogeneity of turbulent air motions is common within thunderstorms even though the mean structure may be relatively steady, as shown in Part II.

The primary storm updraft exhibited very low magnitudes of turbulence at low levels. At increasing heights, the updraft exhibited increasing levels of turbulence which peaked at mid-levels in the vicinity of an updraft/downdraft shear zone. Here, maximum estimated $\Delta V_r/\Delta R$ and $\epsilon$ values exceeded 30 $\times 10^{-3}$ s$^{-1}$ and 0.15 m$^2$ s$^{-3}$, respectively, during the intense storm stages. The magnitude of these maximum values can be compared to other values presented in previous literature. Using similar radar techniques, Frisch and Strauch (1976) measured peak dissipation rates of 0.36 m$^2$ s$^{-3}$ within a northeast Colorado thunderstorm.[1] However, these $\epsilon$ values fall below $\epsilon$ estimates of 1.0 m$^2$ s$^{-3}$ derived from aircraft measurements of turbulence within severe Oklahoma storms. Since aircraft and Doppler radar may not measure the same scale of turbulence, the

[1] These were derived using the universal constant $A = 0.53$ valid for one-dimensional spectra.

validity of such a comparison awaits verification of simultaneous Doppler radar and aircraft measurements of $\epsilon$.

The levels of turbulence generation and the maximum intensity of turbulence correspond well to levels at which the greatest differences between storm updraft momentum (horizontal and vertical) and environmental momentum occur. Moreover, in these same regions strong vertical divergence of vertical momentum suggests that vigorous dynamic entrainment of low-valued $\theta_e$ air initiates downdrafts which, in turn, create locally enhanced shear between updrafts and downdrafts. The mixing of low-valued $\theta_e$ downdraft air with high-valued $\theta_e$ updraft air further generates turbulence by buoyant production. Thus shear and buoyant production operate together in the cloud environment to generate intense levels of turbulence.

The temporal behavior of turbulence within this storm implies that measurements of $\epsilon$ and $\Delta V_r/\Delta R$ can yield indications of relative storm intensity. Observed peaks in turbulent activity paralleled peaks in storm vigor and updraft strength. Patterns of $\Delta V_r/\Delta R$ especially exhibited a striking decrease in strength and areal coverage as the storm weakened. Such a decrease is attributed to decreased activity of large turbulent eddies, as well as diminution of grid-resolvable mean wind gradients produced by vertical exchanges of horizontal momentum and strong updraft gradients. It is tentatively hypothesized that reduced wind gradients, along with decreased mass entrainment due to weaker updrafts, diminished the rate of turbulent kinetic energy generation by mechanical and buoyant production. It would be desirable to obtain finer temporal and spatial resolution of variance and radial velocity patterns over a complete storm life cycle to more accurately establish the origin, behavior and significance of turbulent motions.

*Acknowledgments.* The authors gratefully acknowledge Ms. Polly Laun Cletcher for typing of the manuscript. Mr. Andy Johnston and Mr. Harold Frank are recognized for programming assistance and discussions in data processing. The authors thank Drs. Earl Gossard and William Moninger for discussions concerning the second moment-dissipation relationship, and also benefited from discussions with R. Banta and C. Chen. Several anonymous reviewers are recognized for suggesting improvements in the manuscript. Data processing was performed on the National Center for Atmospheric Research (NCAR) CDC7600 computer. NCAR is sponsored by the National Science Foundation (NSF). This research was supported by the NSF under Grants ATM76-88361 and ATM79-08297, and by the National Aeronautics and Space Administration under Grants NSG-5011 and NSG-5341.

## REFERENCES

Auer, A. H., and J. D. Marwitz, 1968: Estimates of air and moisture flux into hailstorms on the High Plains. *J. Appl. Meteor.*, **7,** 196–198.

Battan, L. J., 1975: Doppler radar observations of a hailstorm. *J. Appl. Meteor.*, **14,** 98–108.

——, 1980: Observations of two Colorado thunderstorms by means of a zenith-pointing Doppler radar. *J. Appl. Meteor.*, **19,** 580–592.

——, and J. B. Theiss, 1973: Wind gradients and variance of Doppler spectra in showers viewed horizontally. *J. Appl. Meteor.*, **12,** 688–693.

Byers, H. R., and R. R. Braham, 1949: *The Thunderstorm.* U.S. Govt. Printing Office, Washington, DC, 287 pp.

Cotton, W. R., R. L. George and K. R. Knupp, 1982: An intense, quasi-steady thunderstorm over mountainous terrain. Part I: Evolution of the storm-initiating mesoscale circulation. *J. Atmos. Sci.*, **39,** 328–342.

Donaldson, R. J., Jr., and R. Wexler, 1969: Flight hazards in thunderstorms determined by Doppler velocity variance. *J. Appl. Meteor.*, **8,** 128–133.

Frisch, A. S., and S. F. Clifford, 1974: A study of convection capped by a stable layer using Doppler radar and acoustic echo sounders. *J. Atmos. Sci.*, **31,** 1622–1628.

——, and R. G. Strauch, 1976: Doppler-radar measurements of turbulence kinetic energy dissipation rates in a northeastern Colorado convective storm. *J. Appl. Meteor.*, **15,** 1012–1017.

Grandia, K. L., and J. D. Marwitz, 1975: Observational investigations of entrainment within the weak echo region. *Mon. Wea. Rev.*, **103,** 227–234.

Heymsfield, A. J., D. N. Johnson and J. E. Dye, 1978: Observations of moist adiabatic ascent in northeast Colorado cumulus congestus clouds. *J. Atmos. Sci.*, **35,** 1689–1703.

Knupp, K. R., and W. R. Cotton, 1982: An intense, quasi-steady thunderstorm over mountainous terrain. Part II: Doppler radar observations of the storm morphological structure. *J. Atmos. Sci.*, **39,** 343–358.

MacPherson, J. I., and G. A. Isaac, 1977: Turbulent characteristics of some Canadian cumulus clouds. *J. Appl. Meteor.*, **16,** 81–90.

Panchev, S., 1971: *Random Functions and Turbulence.* Permagon Press, 444 pp.

Sand, W. R., 1976: Observations in hailstorms using the T-28 aircraft system. *J. Appl. Meteor.*, **15,** 641–650.

Sirmans, D., and R. J. Doviak, 1973: Meteorological radar signal intensity estimation. NOAA Tech. Memo. ERL-NSSL-64, 30 pp.

Sloss, P. W., and D. Atlas, 1968: Wind shear and reflectivity gradient effects on Doppler radar spectra. *J. Atmos. Sci.*, **25,** 1080–1089.

Srivastava, R. C., and D. Atlas, 1974: Effect of finite radar pulse volume on turbulence measurements. *J. Appl. Meteor.*, **13,** 472–480.

Steiner, R., and R. H. Rhyne, 1962: Some measured characteristics of severe storm turbulence. National Severe Storms Project Rep. No. 10, U.S. Weather Bureau, Washington, DC, 17 pp.

Sweezy, W. B., 1978: Comparison of maximum entropy method estimation of Doppler velocity moments with conventional techniques. *Preprints 18th Conf. Radar Meteorology,* Atlanta, Amer. Meteor. Soc., 401–404.

Tripoli, G. J., and W. R. Cotton, 1980: A numerical investigation of several factors contributing to the observed variable intensity of deep convection over South Florida. *J. Appl. Meteor.*, **19,** 1037–1063.

Warner, J., 1970: The microstructure of cumulus clouds. Part III. The nature of the updraft. *J. Atmos. Sci.*, **27,** 682–688.

——, 1977: Time variation of updraft and water content in small cumulus clouds. *J. Atmos. Sci.*, **34,** 1306–1312.